

# Electrostatic accelerated electrons within information horizons exert bidirectional propellant-less thrust

Becker, F. M.      Bhatt, Ankur S.

June 16, 2019

## Abstract

During internal discharge (electrical breakdown or field emission transmission), thin symmetric capacitors accelerate slightly towards the anode, an anomaly that does not appear obvious using standard physics. The effect can be predicted by core concepts of a model called quantised inertia (also known as MiHsC) which assumes inertia of accelerated particles, such as electrons, is caused by Unruh radiation. This discrete Unruh radiation forms standing waves between the particle's boundaries to a Rindler horizon and a confinement horizon, which are established based on special relativity in concert with quantum mechanics. Electrons accelerate toward the anode and are assumed to encounter an inhomogeneous Unruh radiation condition causing a force suggested by a modification to their inertial mass. To conserve momentum, the overall mechanical system moves in the direction of the anode. This resulting force is assumed to be caused by an energy gradient in between the confinement and the Rindler zone and its equation is derived directly from the uncertainty principle. Various thicknesses of discharging capacitors are compared to show the agreement between the experimental findings and a virtual particle oscillation associated with a standing wave energy gradient hypothesis. The preliminary correlation results are encouraging.

**Keywords:** electric propulsion, Unruh radiation, Rindler Horizon, electron discharge thrust, quantum vacuum thruster, QVT, quantised inertia, imFaB, discrete virtual particle spectrum, quantum foam, information horizon energy gradient

## 1 Introduction

It was experimentally observed (Becker F.M. 1990) that a thinly charged parallel plate capacitor, supplied with high voltage values of 5 kV DC - 10 kV DC, exerted an unexpected observable force towards the anode. This anomaly was only detected while using dielectrics with low dielectric breakdown strength, however it progressively disappeared when increasing the dielectric breakdown voltage (and the material thickness.)

Such phenomenon was initially disregarded as a likely artifact, but a few years later, additional considerations lead to the speculation that electric discharge could have been the cause of the anomaly, however no further testing was conducted. The initial observations suggested that stronger dielectrics, with their enhanced performance in withstanding voltage, would not lead to an observable effect while the electric discharge (breakdown of insulation leading to partial/full discharge or field emission) could be responsible for the appearance of the phenomenon. In addition, Talley R.L. [11] had described a comparable anomalous observation which might have been caused by accelerating electrons or electric charges, further reducing the likelihood of a simple artifact.

While conducting a variety of capacitive discharge experiments in 2017/2018 and additional battery powered wireless experiments in 2019, data was collected during field emission and insulation breakdown discharge events of parallel capacitive charged plates. Data was collected for very short capacitor plate distances. Additionally, the collected data investigated any correlation between any anomalous force and the accelerated mass and an anomalous force with the decrease of the capacitor electrode distance, while keeping the accelerated mass constant.

## 2 Method

### Experimental setup and test apparatus

#### 2.1

Electrons are an easy-to-control option to achieve high acceleration of particles. Also with reference to the anomalies characterized by Talley R.L. [11], such conditions are observed as potentially relevant. The high field strength achieved in the thin electrode separation can provide constant electron accelerations in the magnitude of  $10^{19}$  [ $\text{m s}^{-2}$ ] (acceleration equals the fundamental electric charge divided by mass of an electron multiplied with voltage divided by the electrode distance). This acceleration would be associated directly to a Rindler horizon distance and with a presumed maximum wavelength [8] of the spectrum of Unruh radiation. This is done by considering only allowed radiation with nodes at the boundaries [7] which are able to be attenuated with conductive plates in the range of normal engineering practice. The strong electric field releases electrons through the high-field emission effect [5]. With the objective of achieving higher force values, the material was heated so that the energy value required by the electric field for electron transmission could be lowered [9] (Schottky effect): in other words, warming the material allowed to increase the discharge of electrons using the same strength of the electric field. The application of heat enables thermionic emission as well as supplying some electrons with at least the minimal energy required to overcome the barrier force holding them in the material structure (reference to the concept of work functions of materials).

#### 2.2

Capacitors were designed with polyethylene dielectric materials. Other materials, such as paper, glycerin, and porous plastics, were also tested but this resulted in discharges involving ionic charge flow which traveled in the opposite direction of the electron

flow hindering the effect. Furthermore, some materials are prone to cavities (atmospheric voids) that introduce partial discharges [3] where electron avalanches generate ion current contribution inside the hollow space. Additionally, paper insulators were ineffective in generating measurable thrust effect since the atmospheric electron avalanches (see Paschen law [2] for breakdown voltage vs distance) would release secondary electrons but also induce ionization as well. Overall, the experimental data seem to validate that, for the design and manufacturing of a thruster device using the observed phenomenon, a vacuum propagation of the accelerated electrons, or the application of semiconductor cathode arrays, could be the most effective method to obtain a controllable effect.

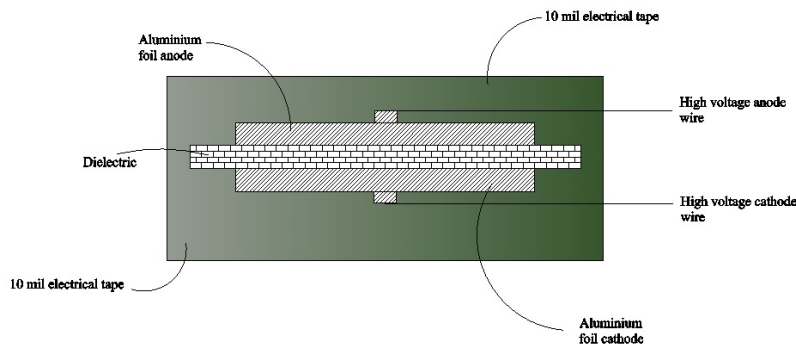


Figure 1: General prototype construction

Remark: Depending on the actual insulator thickness (as described in this document) it can be assumed that currents slightly below  $1 \mu\text{A}$  are essential to generate thrust forces to trigger the load sensor (i.e. LEADZM B300T digital scale with typical sensitivity of 0.001 mg and error of 0.003 mg).

Considering the available power sources (5 kV DC, 10 kV DC), the electric field strength between the capacitor plates would be estimated to be below the actual effective tunneling field strength required to provide a sufficiently reliable current density to support the effect. Therefore, the homogeneous field character had to be enhanced into a partial inhomogeneous field to increase the field strength by altering the smooth flat shape of the emitting surface and adding sharper edges (reduced radius of an emitting surface corresponds to increase in the electric field strength as similar to a concept of a needle cathode). This was done by cutting into the electrode or by using sandpaper on the cathode surface to facilitate field emission. This was done using a precision knife applying a high number (hundreds) of small cuts on the electrode or by surface treatment with a fine sandpaper. Obtaining a sharp edge contributes to a higher field strength through the creation of inhomogeneous electric fields, in analogy with a needle electrode. If only homogenous fields are used, this (cold) emission would need an electric field strength to begin on the order around  $10^7$  to  $10^8$  [V/m].

For some tests, typically associated with higher thrust force values, the overall capac-

itor was preheated for testing up to approximately 50 °C before placing the device onto the measurement apparatus. This also denotes that testing attempts at low ambient temperatures without pre-heating may lead to a thrust force too low to be detected.

### 2.3

Confirmation tests in soft vacuum were conducted by placing the capacitor inside a sealed container, shielded by wrapping it in a conductive (grounded) outer layer. Such tests yielded results comparable, in terms of average, with the set-up of open air. Nonetheless the corresponding spread standard deviation of the data points recorded was lower for the soft vacuum ( $\sim 20$  torr) during experimental tests.

### 2.4

The supply wires had been twisted [1] to reduce electromagnetic effects (Lorentz force etc.). This operation was performed very carefully to prevent the generation of torque onto the system. Nevertheless, the order of magnitude of theoretical torque contribution was estimated to be sufficiently low for not altering the observable phenomenon, reducing the concerns related to any possible residual torque. Moreover, the supply conductors were routed to an adequate distance ( $\sim 200$  mm) to prevent electromagnetic field disturbances on the load cell of the digital scale. Field disturbances to the load cell leading to the corruption of displayed measurements were observed in the range less than  $\sim 50$  mm around the digital scale. The metal film shunt resistors used for voltage measurements to determine the electric current had a 1 % error tolerance while the probes used were approximately 2 %. The scope used for electric current measurements was a Keysight DSO1052B Oscilloscope-2 Channel-50 MHz.

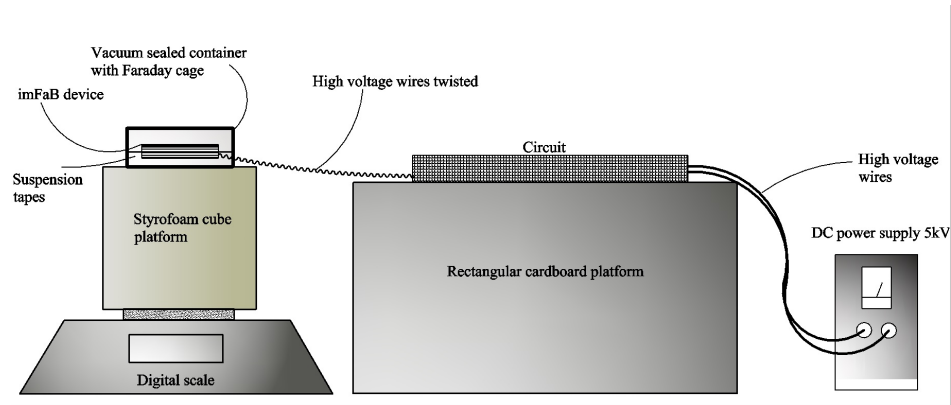


Figure 2: Experiment setup

## 2.5

The dielectrics had been tightly fit between the conductive surfaces to minimize the air presence. If a considerable air layer is present, in fact, this could lead to ions traveling in the opposite direction of the electrons due to avalanche processes by direct arcing, dampening the amplitude of observed thrust. As previously explained, this might also occur in certain materials when the high-field strength introduces partial internal discharges in material porosities where electrons as well as secondary avalanche electrons can generate positive charged ions. Furthermore, when glow-discharge/stronger arcing occurs, the acceleration voltage over the capacitor would decrease significantly, down to a typical  $\sim 30V$  typical arc voltage level. In this condition particles, instead of being linear accelerated, would be subject to Langmuir waves, thus (plasma) rapid oscillations of the electron density related to the instability in the dielectric function. The experiment was consequently set up to minimize the risk of these occurrences (which sometimes had been observed with the test device accelerating slightly towards the earth regardless of the polarity).

## 2.6

It was essential to protect the measurement tools/devices of the circuit from the influences of voltage transients that could occur in a situation where the insulation resistance of the capacitor would drop significantly. In such cases, the shunt resistor would carry a higher voltage due to the voltage divider characteristic of the circuit (more precisely, this is related to the capacitor insulator experiencing a reduced resistance). The circuit, see Fig. 3, does not employ any preventive measures for such phenomena, with regards to the application of transient surge protective devices. However, a large resistor (compared to the shunt resistive value) in series with the shunt could be introduced to serve as a voltage divider in case of insulation failure. Such transient effects are seen more likely when the field emission current increases. In addition, heating the dielectric insulation material could potentially reduce the insulation resistance of the dielectrics.

## 2.7

An alternative to the 5 kV DC commercial power source was also used. A conventional flyback transformer with a maximum output slightly above 10 kV DC has been utilized for voltage sweeping during the experiments to vary the electron's acceleration. The flyback transformer was supplied in the primary winding by a conventional DC power supply. The output voltage characteristic has been interpolated by the input/output data specifications of the flyback manufacturer for computations. Additionally, the electric circuit was rectified (smoothed) by a tank capacitor to provide a stable supply voltage to the capacitor.

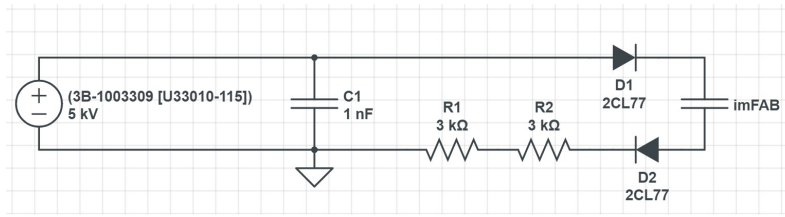


Figure 3: Functional circuit

## 2.8 Wireless Setup

During additional testing in January 2019, the entire thruster system was placed inside a grounded faraday cage with an inner insulation barrier. Only DC supply wires exited the cage and were connected to a battery-onboard. These low voltage DC supply wires ran vertically and twisted until terminal connections at the flyback transformer. All high voltage components were located inside the cage without any atmospheric exposed HV supply conductors. The thruster box, including the battery power supply and high voltage source, was placed on the scale and the center of gravity effects were addressed before measurement. Additionally, a wireless relay was installed on the top of the cage to turn the system on and off remotely without physical access. Signal conductors were routed to the measurement circuit (shunt to the oscilloscope). The effect device ON voltage level was fixed to around 5kV which was measured from the output of the flyback transformer with smoothing capacitor in parallel.

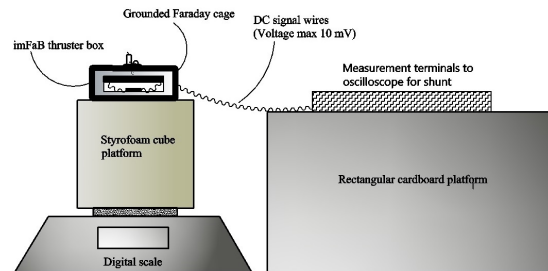


Figure 4: Wireless setup

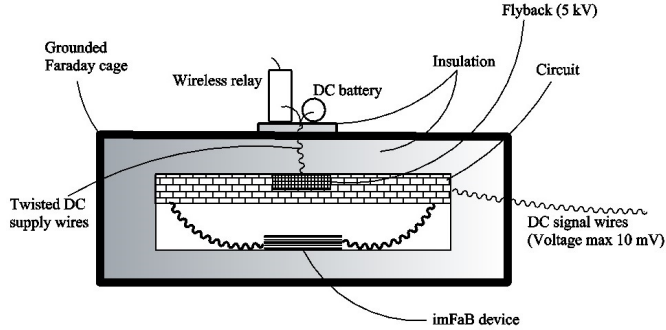


Figure 5: Thruster device

## 3 Results

### 3.1 Thrust observation versus electrode distances

The electrode distance had been varied and the force monitored. Since the discharge current is dependent on the Schottky effect (field enhanced thermionic emission), which is determined not only by the electric field strength but also by the heat of the surface, the actual current for each data point statistically fluctuates. Consequently the graphs illustrating the results of the current measurements are normalized to a constant set-up (same charge amount, same accelerated mass). These explained predictions also correlate to a proposed hypothetical model of a quantum oscillator which provide a discrete spectrum where, within this document, Unruh radiation is generated by a Rindler horizon information boundary by acceleration.

Note: accelerated (accumulated) mass corresponds in value determined as the electric current multiplied with the mass of an electron and divided by the elementary charge.

If a constant current (an accelerated mass of electrons) is provided, the reduction of the distance between the electrodes cause the thrust force effect to exponentially increase in value. The electrodes distance is equivalent to the dielectric insulation thickness, and in the remainder of the paper the two dimensional characteristics are used interchangeably being equal in value.

The first sub-experiment was conducted with different insulator thicknesses, between  $13 \mu\text{m}$  to  $80 \mu\text{m}$ , which influenced the acceleration experienced by the electrons. The diameters of the capacitors ranged from  $2.5 \mu\text{m}$  to  $5 \mu\text{m}$  and a total of 266 data points were collected. The measured current value was standardized (as fluctuating under the effect of field emission) to a normalized current level of an arbitrary  $10 \mu\text{A}$ . The accelerated voltage was tuned to 5 kV for all measurement points while testing different insulation thicknesses. The acceleration voltage of approximately 5 kV corresponds to an electric acceleration inside the insulator thicknesses on the order of  $10^{18}$  to  $10^{19} [\text{m s}^{-2}]$ .

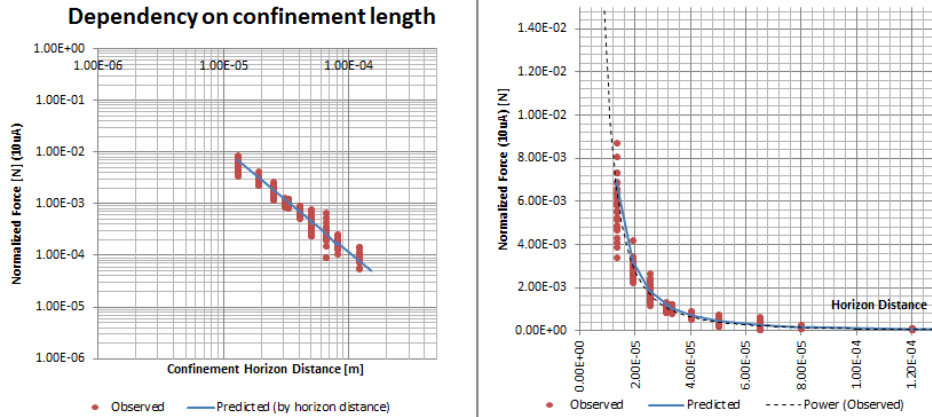


Figure 6: Normalized force versus distance

While altering the electrode’s distance, it is observed that the recorded force follows a linear trend in a logarithmic view. Hence the trend is attributed to an exponential increase of force by a linear reduction of the electrodes distance. Later, this will be defined as a horizon distance or confinement of the seeing zone (an expression by McCulloch, the propagation direction) which is in front of the accelerating particle.

Unless otherwise specified, data points of individual graphs are considered an absolute value since these points correspond to both directional scenarios (force towards measurement scale and opposite). The anode of the capacitor pointing upwards was associated to an upward acceleration while the anode pointing downwards was associated to a downward acceleration. This remained valid as long as no reversal force mechanism was introduced (see section 3.3 for details).

In Fig. 7 the actual force direction shows dependency on the accelerated mass measured with the proportional electric current. The symmetry of the data points illustrates that the observed force appears independent of influences of gravity, ionic winds, thermal buoyancy and other such artifacts. Additionally, several tests have been conducted in low vacuum using a simple sealed container (data points identified as ‘vac’ in the attached graph), showing a trend line characterized by a lower standard deviation compared to the open-air tests. The top half of graph where force is positive correlates with the anode facing upwards while the bottom portion of the graph is associated with the anode facing downwards.

Note: Vacuum measurement of the median thrust observations (conducted on the 33  $\mu\text{m}$  capacitor) is associated to a 8 % standard deviation. Other non-vacuum measurements are in the range from 11 % (33  $\mu\text{m}$ ) to higher values of 30 % (50  $\mu\text{m}$ ). The vacuum appears to have stabilized the effect from 12 % ( $\sigma = 1.2 * 10^{-4}$  N at mean of  $1.0 * 10^{-3}$  N) down to 8 % ( $\sigma = 8.7 * 10^{-5}$  N at mean of  $1.1 * 10^{-3}$  N).

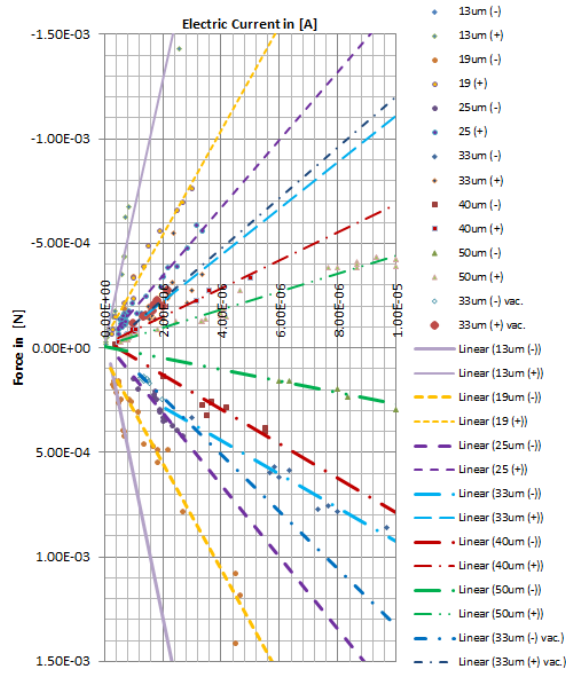


Figure 7: Force versus Current

The operational characteristic of the identified thrust effect shows a linear dependency with the amount of accelerated electron mass and increases exponentially with linear decrease of electrode distance.

**Note:** The graph shows that for thicker insulators the observed thrust was greater when the anode (+) was oriented on the top of the capacitor. This fact could be correlated with a slight influence of buoyancy determined by the preheating which is required to obtain higher force values.

As advised by Prof. Dr. M. Tajmar, the capacitor plates were tested in vertical position in the attempt to have a null effect that would confirm the absence of external perturbations. This verification test was conducted obtaining a null force (instead of diffuse force directions), confirming the validity of the experimental set-up and the directional attribute of the thrust.

The graph hereunder shows similar trend lines compared to the estimated power consumption.

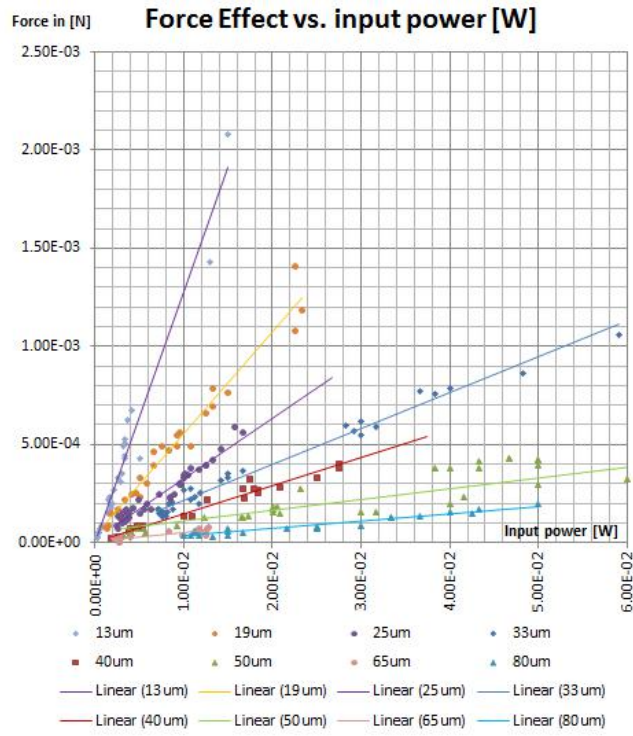


Figure 8: Force versus input power

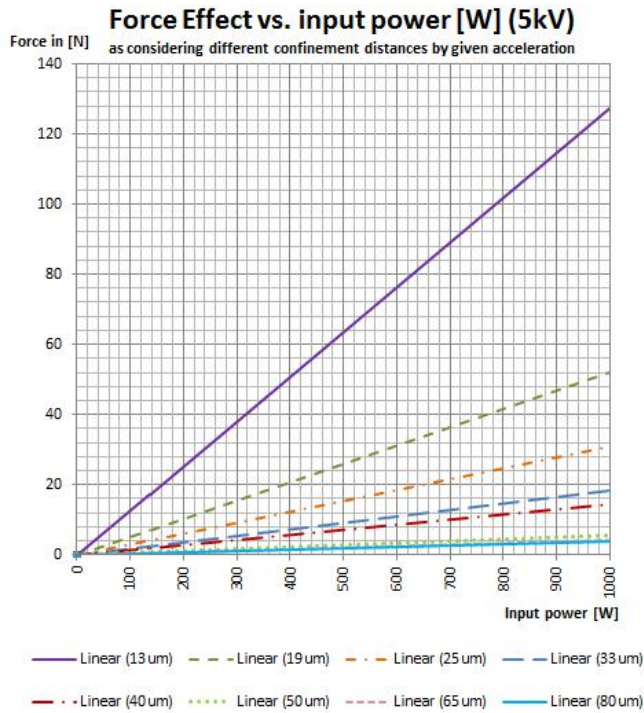


Figure 9: Force versus input power extrapolated

The same graph can be extrapolated to show the force versus power ratio of a scaled up thruster device up to 1 kW input power.

Remark: Lower thrust performance on thicker insulators is associated with a higher standard deviation (as visible in the lower left corner of the graph). Higher force values are associated with applied heat in combination with shorter electrode distances. From a practical perspective, this is an important evidence because the output of a high thrust device should be easier to control.

Furthermore, the effect and operational thrust characteristics can be displayed by combining the square root of the accelerated mass and the energy gradient between the Unruh baths into one factor. The linearity in the logarithmic scale shows the combined dependency of the elements of the mass and Unruh radiation energy related to the accelerating particle.

**Note:** This view provides the advantage to compare all electrode separation distances in one combined graph.

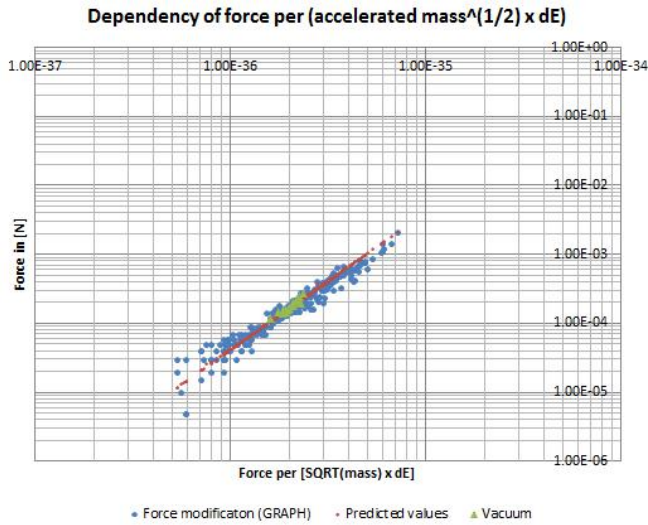


Figure 10: Force versus accelerated mass and energy

The use of the low vacuum container, where the thrust device is placed and shielded inside, appears to stabilize the measured data points versus prediction.

### 3.2 Thrust versus change of acceleration voltage as proportional to the Rindler distance

The Rindler distance is determined by the electric field strength and acceleration. Electric acceleration is yielded by the following: electric field strength multiplied by the elementary charge divided by electron mass  $a_e = Eq/m_e$ . Here the electric field strength is determined by voltage divided by electrode distances. In reference to the works of M.E. McCulloch, the Rindler distance had been calculated by the square of the speed of light divided by the acceleration  $R = c^2/a$  [6].

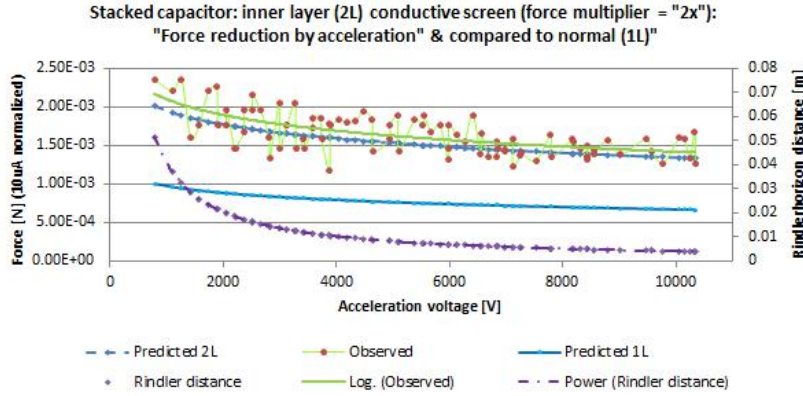


Figure 11: Force versus acceleration voltage for double layer capacitor

As increased voltage was applied, a slight decrease in normalized force occurred. Voltage was swept from 1 kV to approximately 10 kV and a total of 97 data points were collected. Furthermore, capacitor elements were stacked in series in the attempt to obtain a force multiplier factor. With respect to the reduction of the force with an increase in acceleration voltage, it is evident that an increase of the effect corresponds to the reciprocal of the kinetic energy of the accelerated electrons (the effect is reduced with increasing kinetic energy of the particles).

With respect to the force multiplication for these measurements, instead, the preference was to use a modified capacitor which incorporated an additional inner conductive floating material similar to the cathode/anode foil between the two insulators. Such an arrangement represents a series capacitor meaning that the voltage was approximately halved. Assuming that the supply current yielded the same volume of electrons, the results suggest that the electrons got accelerated twice. The prediction method, (see section 4) using the amount of events for each accelerated particle, would only yield about half of the measured force value. Doubling the amount of events, since the electron gets re-accelerated from the inner floating plate, resulted in a prediction that would be in compliance with the observation.

It should be noted that by using the proposed physical model, a reduction of the Rindler distance compared to the confinement zone (located in front of the accelerating particle), would reduce the number of unshared wavelengths hence, would influence the energy gradient. This influence resulted in a decrease in  $dE$ , which was the energy difference between the potentials of Rindler zone and propagation area.

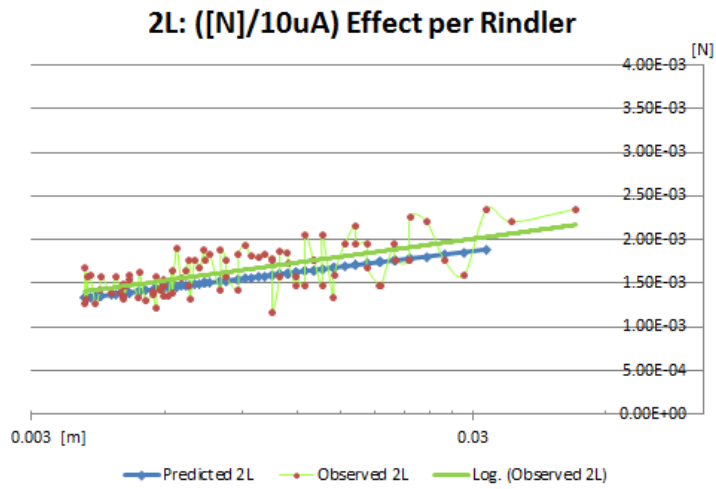


Figure 12: Force versus Rindler distance at  $10\mu A$

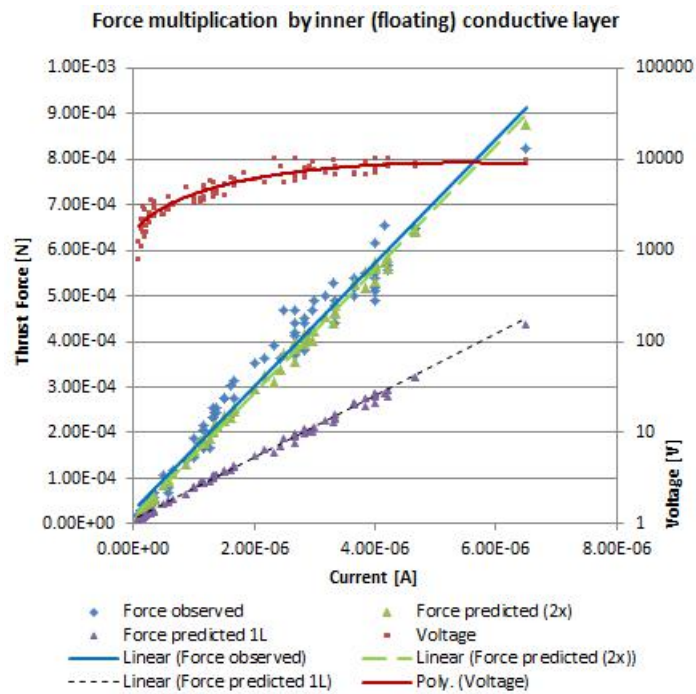


Figure 13: Force versus current for double layer capacitor

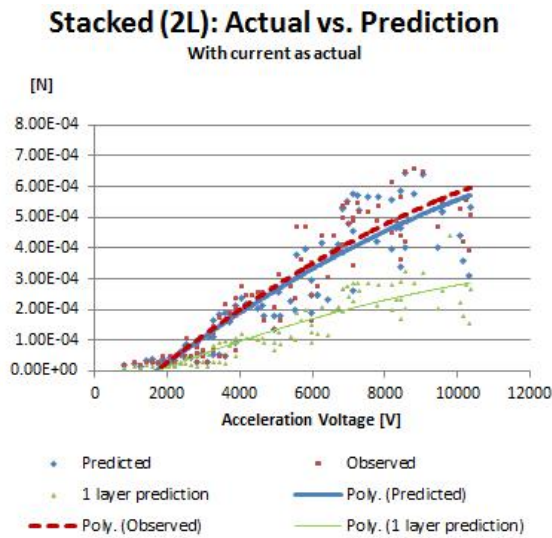


Figure 14: Force versus voltage for double layer capacitor

For reference Fig. 15 illustrates the overall weight modification which was observed during the various experiments.

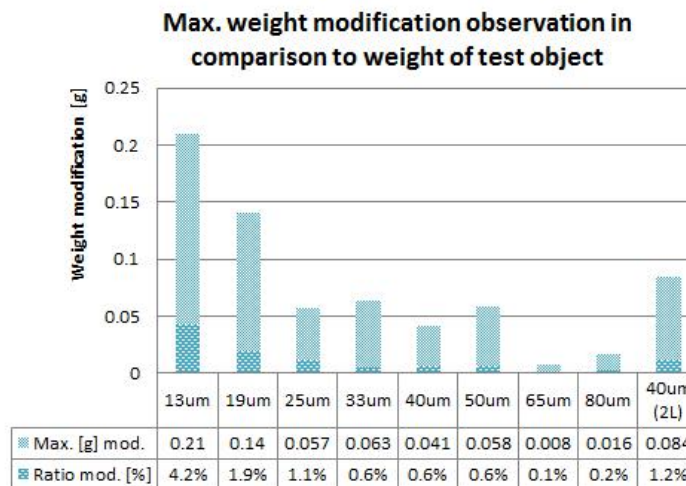


Figure 15: Maximum weight modification for all capacitors

An interesting piece of evidence was that some capacitors showed a lower performance in the number of accelerated particles: such performance was detected by measuring a lower electric current. This figure has the main purpose of illustrating the highest amount of force achieved with the different electrodes distances.

### 3.3 Altering Rindler zone with insertion of conductive attenuation materials

Additional tests performed (144 data points) resulted in the identification of a reversal in directional force. When a particle or object is accelerated, a Rindler horizon forms behind it. Therefore, assuming the existence of this information boundary zone, an experiment had been conducted by inserting a conductive material into the zone. According to the skin depth's equation (see Appendix B), it is assumed that even a thin material could attenuate up to the maximum wavelength of the standing waves with nodes at the horizon as would be allowed by the Rindler distance.

Four different behaviors were identified:

1. When the thickness of the cathode was extended before the rindler horizon,  $R$ , the thrust effect appeared to be linearly reduced (slope of  $-2R$ ) with respect to the increased elongation of the cathode.
2. When a conductive material, electrically insulated from the cathode, was inserted into a certain area behind the cathode but before  $R$ , a full force reversal (compared to the original observed effect) was observed.
3. When a conductive material, electrically insulated from the cathode, was inserted a sufficient distance behind the cathode and beyond  $R$ , a normal compared effect was observed.
4. When the thickness of the cathode was extended beyond  $R$ , a full force reversal (compared to the original observed effect) was observed.

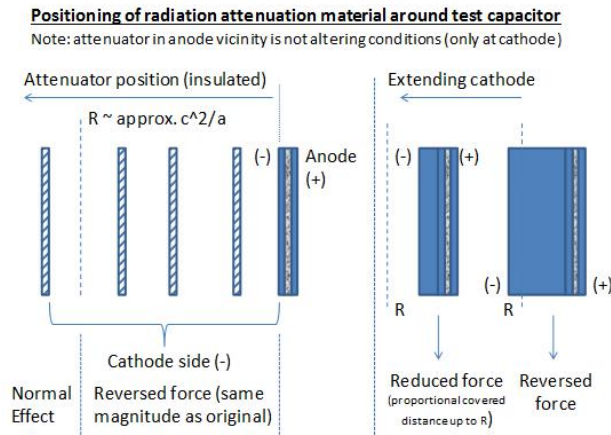


Figure 16: Strategic positioning of radiation attenuation materials

Suspecting that the forces observed are linked to the Unruh-like radiation experienced by the capacitor during the electrons acceleration, several additional tests were performed in the attempt to dampen shorter wavelengths thus influencing the generated

force. This was done introducing an attenuation material, aluminium sheet on the order of a few tenths of a millimeter, at several distances from the surface of the cathode.

After numerous tests, it was discovered that the force could be reversed with same value of the original force at all distances less than the rindler horizon  $R$  when the attenuator material was electrically insulated from the cathode. When placing the attenuator past the distance  $R$  (which corresponds to approximately to a length equal  $c^2/a$ ) led to a sudden change of force direction. This change in direction with the attenuator sheet the beyond the rindler horizon led to the sudden recovery of the original force direction (towards anode equal to electron propagation path).

Furthermore it was observed that an extension in thickness of the conducting cathode was not leading to a force reversal but to a reduction of the force. This was estimated as being proportional to the covered space between original position of the cathode surface and the rindler distance,  $R$ . It should also be noted that there could be an exponential decrease since data points between  $0.5R$  and  $R$  were not in the range of the measurement device. Finally, if the cathode thickness exceeded  $R$  a force reversal was established with the same magnitude of the full normal effect (propagation toward the anode).

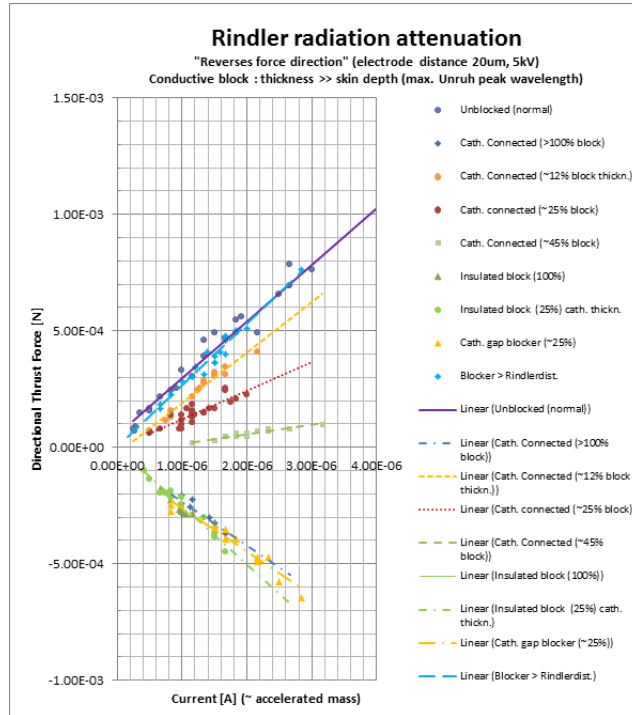


Figure 17: Force [N] versus current for various blockers

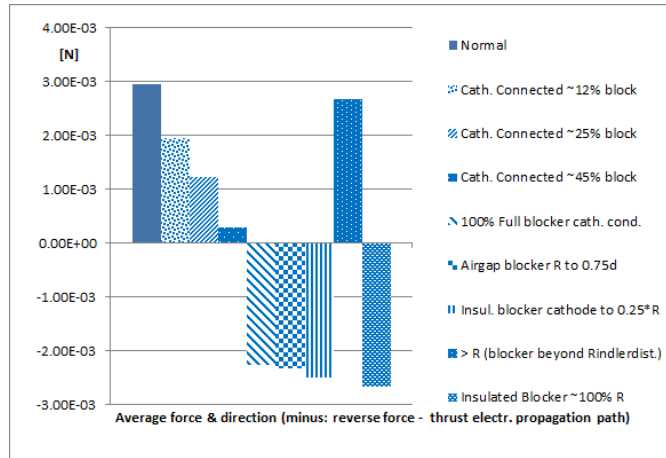


Figure 18: Force [N] for different blockers with data measurements averaged

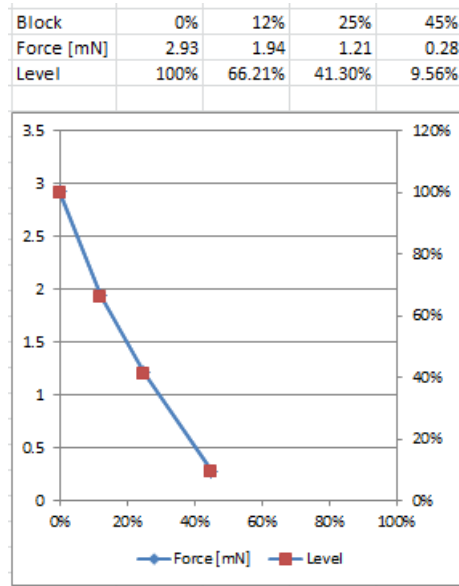


Figure 19: Force [N] reduction for blockers with data measurements averaged

The observation of reversing the accelerated direction, with same level of the original thrust force, might be seen as an effect involving an accelerated frame of reference. During the original effect, the Rindler horizon propagated together with the electrically accelerated electron (co-moving) and the Rindler horizon moved as the electron traveled. Looking into this scenario it can be considered as one accelerated inertial reference frame which is initially accelerated on the level of the electric acceleration.

Physical standard models describe this (accelerated) situation by introducing one fictitious/pseudo force (adding on the electrical acceleration force vector) which denotes an additional thrust acceleration vector. As per Newton's third law, forces only exist in pairs and this inertial force on the electron's co-moving inertial accelerated frame could be assumed to be directed opposite to the accelerated direction of electron propagation. In the frame of the external observer, this fictitious/pseudo force could change the acceleration direction since the actual effect force is cancelled by the causal blocking of the Rindler horizon. In this model the other pair component of the cancelled pseudo force would remain valid and directs the acceleration direction leading to a reversal. This might happen because the energy of Rindler zone could be assumed to stay present/valid, but is not able to propagate to provide an accelerative force; hence, the inertial force pair stays in existence.

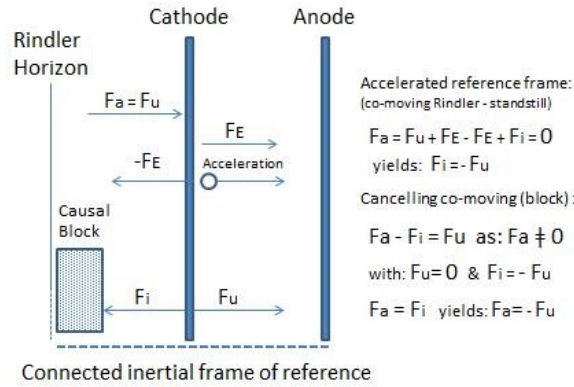


Figure 20: Inertial frame force

### 3.4 Wireless Experimental Results

The new battery-powered onboard wireless setup resulted in a convergent force trend-line with the previous data collected for 20 um distance (October 2018). Both devices had a supplied voltage of 5 kV. Generally, smaller thrust values from lower current values were found due to the lower ambient temperature conditions and lack of heat applied to the imFaB device. Artificial heating to increase electric current was avoided to prevent heat trapped inside the closed grounded Faraday cage . This could have resulted in buoyancy errors.

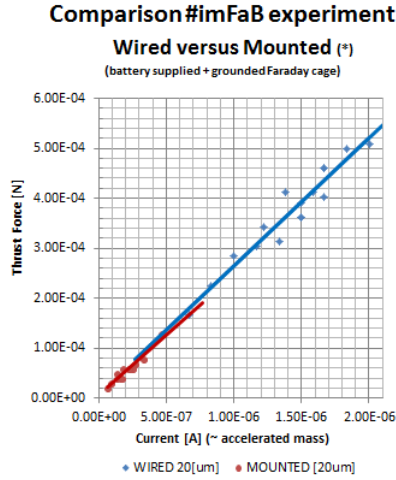


Figure 21: Wireless

## 4 Method

In particular the fast/frequent burst electric discharge thrust effect (named FBeDT) is not only associated to capacitors, where the thrust towards the anode is caused by effects assumed from the high voltage supply [10], but is a more general effect that uses capacitors as an experimental mechanism to accelerate particles (with a defined accelerated condition). The electric acceleration is used to observe an effect caused by propagating electric charges (particularly electrons discharging in insulation breakdown and field emission tunneling into solid materials) in very high electric field strengths resulting in hyper-accelerating electrons. It also should be noted that the thrust effect (in the propagation direction of the accelerating particle) is reversible not only by changing polarity (per reversing the acceleration direction), but by altering conditions in the space behind the accelerated electrons, namely, between the Rindler horizon and the cathode. The capacitors (in general breakdown or field emission mode) are used as a mechanism to accelerate particles with known particle mass and can be achieved within very short electrode distances.

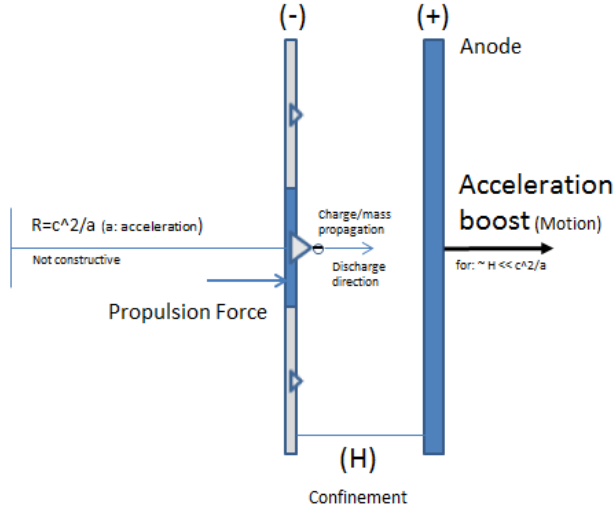


Figure 22: Force diagram of thruster

According to the latest understandings in physics it is considered probable that not only singularity horizons [4] but also Rindler horizons generate thermal radiation [12] [13]. Recent developments in theoretical physics [7] [8] assume such radiation as confined in boundaries would exist quantised with wave nodes at the horizons. Under normal conditions an accelerated particle experiences a maximum thermal Unruh radiation (peak wavelength) of approximately 8 times the maximum wavelength as confined in the Rindler horizon zone. This situation causes inertia [7] [8].

In order to alter the inertia of an object, it is assumed that it would be possible to reduce the maximum Unruh wavelength, or equivalent associated harmonic oscillations by virtual particles. This could be established by information loss at a horizon in the region, in front (propagation direction) of an accelerating object, and therefore, reduces the (discrete, due to nodes at the horizon) spectrum and the total amount of waves allowed in the confinement. Wave attenuation, into a confinement condition, would be accomplished by reducing the distance to the information boundary and would limit the maximum radiation wavelength in front of the accelerated object and the Rindler horizon. If a confinement in the electron propagation path is established with the same distance as the Rindler horizon, an inertia equilibrium situation would be achieved. If the attenuation position is further reduced, more Unruh waves in the propagation zone would be cancelled and the total wave energy (in the zero point field) in front of the accelerating particle would be less available in the Rindler horizon zone. In the case of small particles, this would allow a one dimensional methodology to simulate the conditions.

#### 4.1 Theoretical force model by uncertainty principle

Having documented and demonstrated that an effect exists to generate an anomalous force, the question remains whether this could also work in theory. Begin by using the uncertainty principle  $\Delta x \Delta p = \hbar/2$  and the assumption that by nodes at the horizons

the energy level is fully determined so the  $\Delta x$  would be equivalent to the maximum possible uncertainty in the given boundaries (horizons). In this specific case, there are no rotations/orbits therefore, one will not need to use  $\hbar$  and instead  $h$  will be used since electrons are traveling in a straight path (linear momentum.) Assuming that in a confined space  $\Delta x \Delta p = h$  the confined attenuated energy is  $\Delta E$ , this would result in the summation of the total number of virtual particle oscillation energies down to the Planck length ( $l_p$ ). As the linear momentum ( $\Delta p$ ) is equivalent (and determined) as  $\Delta E = \Delta pc$ .

Use the energy formula for a photon  $\Delta E = \Delta pc$  and substitute in for  $\Delta p = h/\Delta x$ .

$$\Delta E = \frac{hc}{\Delta x} \quad (1)$$

Here the unshared waves from the energy gradient will create a net force on the capacitor. This is due to the fact that the unshared waves only fit at the nodes of the rindler horizon and the cathode. The shared waves in both the Rindler region,  $R$ , and the confinement,  $d$ , will not attribute to any net force.

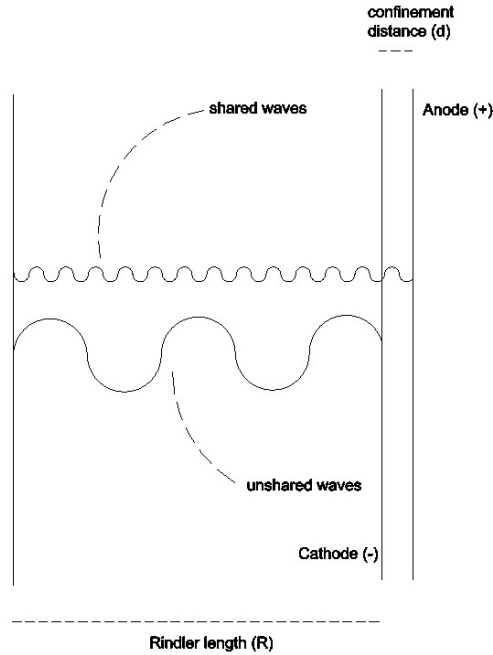


Figure 23: Unshared waves gradient force on capacitor

Plug in for  $\Delta x = kl_p$  in order to count all the waves in the confinement region up to  $N$ . Here  $l_p$  is denoted as Planck length. Additionally,  $N$  represents the number of the fundamental oscillations allowed in the confinement.

$$\sum_{k=1}^N \Delta E_d = \frac{hc}{l_p} + \frac{hc}{2l_p} + \dots + \frac{hc}{Nl_p} \quad (2)$$

Plug in for  $\Delta x = kl_p$  in order to count all the waves in the Rindler region distance ( $R$ ) up to  $M$ .

$$\sum_{k=1}^M \Delta E_R = \frac{hc}{l_p} + \frac{hc}{2l_p} + \dots + \frac{hc}{Ml_p} \quad (3)$$

Now compute the ratio of fractional energy that will be pushing the capacitor. Namely, the ratio  $\frac{\Delta E_R - \Delta E_d}{\Delta E_R}$ .

$$\frac{\Delta E_R - \Delta E_d}{\Delta E_R} = \left( \frac{\frac{hc}{l_p} + \frac{hc}{2l_p} + \dots + \frac{hc}{Ml_p}}{\frac{hc}{l_p} + \frac{hc}{2l_p} + \dots + \frac{hc}{Ml_p}} \right) - \left( \frac{\frac{hc}{l_p} + \frac{hc}{2l_p} + \dots + \frac{hc}{Nl_p}}{\frac{hc}{l_p} + \frac{hc}{2l_p} + \dots + \frac{hc}{Ml_p}} \right) \quad (4)$$

Now write the equation in closed form and simplify.

$$\frac{\Delta E_R - \Delta E_d}{\Delta E_R} = \frac{\sum_{k=1}^M \frac{1}{k} - \sum_{k=1}^N \frac{1}{k}}{\sum_{k=1}^M \frac{1}{k}} \quad (5)$$

Now, replace  $M$  with the total waves in the region  $R/l_p - 1$  which are the total waves in the Rindler region down to Planck length. Also replace  $N$  with  $d/l_p - 1$  which are the total waves in the confinement region. Finally, multiply by  $hc/d$  using (1) to get the total energy gradient of one electron.

$$\Delta E_e = \frac{hc}{d} \frac{\sum_{k=1}^{R/l_p-1} \frac{1}{k} - \sum_{k=1}^{d/l_p-1} \frac{1}{k}}{\sum_{k=1}^{R/l_p-1} \frac{1}{k}} \quad (6)$$

Use the closed form approximation for a harmonic series formula namely,  $\sum_{k=1}^N \frac{1}{k} \approx \ln \frac{2N+1}{2(1)-1}$  for both summations. This yields the same results as applying the Euler-Maclaurin formula for harmonic series, namely  $\sum_{k=1}^k \ln(k) + \gamma + \epsilon_k$  where  $\gamma$  is Euler's constant and  $\epsilon_k$  represents the higher order error terms.

$$\Delta E_e \approx \frac{hc}{d} \frac{\ln\left(\frac{2R}{l_p}\right) - \ln\left(\frac{2d}{l_p}\right)}{\ln\left(\frac{2R}{l_p}\right)} \quad (7)$$

Fig. 24 suggests that a correlation with the physical action exists. The area under the curve represents [J m] which is the units of energy distance or action which is [kg m<sup>2</sup>s].

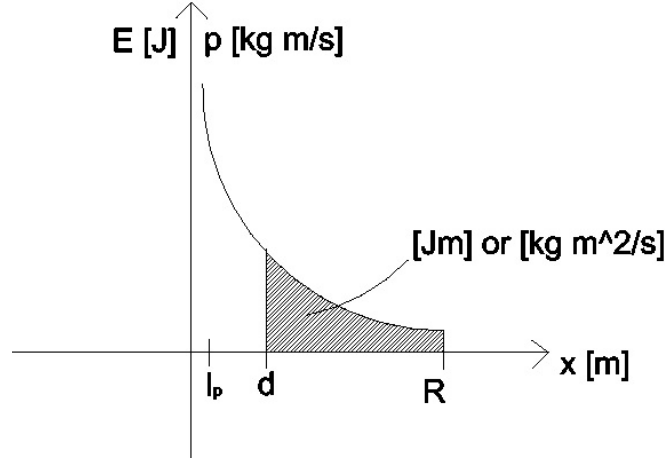


Figure 24: Energy and momentum versus distance

**Note:** Regarding Fig. 24 by conjugate variables, the linear momentum is the overall derivative of the corresponding action with respect to the position. In particular the uncertainty in position (also per quantum hydrodynamics) states that the action is the conjugate variable of the probability density.

Now also notice (7) can be written as the subtraction of two energy regions.

$$\Delta E_e \approx \frac{hc}{d} \left( 1 - \frac{\ln(\frac{2d}{l_p})}{\ln(\frac{2R}{l_p})} \right) \quad (8)$$

Use the change of base formula to obtain the following. This results in the subtraction of two energy regions. Notice the full Rindler region is not used for  $\Delta x$ .

$$\Delta E_e \approx \frac{hc}{d} \left( 1 - \log_{R/l_p} d/l_p \right) \quad (9)$$

Now proceed back from (7) and combine the numerator using property of  $\ln a - \ln b = \ln(a/b)$  for a more simplistic form.

$$\Delta E_e \approx \frac{hc}{d} \frac{\ln(\frac{R}{d})}{\ln(\frac{2R}{l_p})} \quad (10)$$

Now solve for the force  $\Delta F_e = \frac{\Delta E_e}{0.5d}$  by substituting in (8). Notice the distance is to the middle of the confinement. This gradient was identified to be possible by measurement. This gradient might also denote a relation to the superimposed wave functions in a scenario where the average position of the Unruh radiation photons are in the middle of the confinement by Maupertuis's principle. Basically, the momentum of each harmonic oscillation is defined by its node from the information boundary (photons acting similar to an electron in a box scenario). The energy eigenstate has a symmetric probability amplitude therefore, this result leads to the notion that the uncertainty in position is distributed within the zone evenly and henceforth the average position is in the middle of the confinement. On the other hand, looking into a probabilistic density

of the particles over the length of the confinement, one can see that an average low density level (like an energy divergence drain) would be statistically in the middle of a confinement. This might denote that the gradient, as identified, is a probabilistic time averaged parameter.

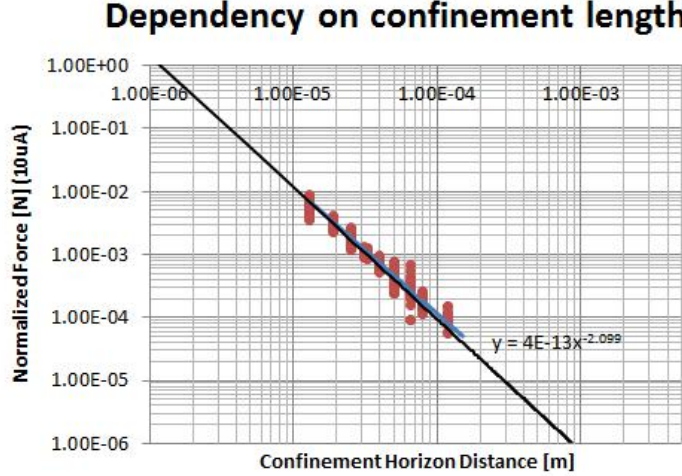


Figure 25: Normalized force versus confinement length

$$\Delta F_e \approx \frac{2hc}{d^2} \frac{\ln(\frac{R}{d})}{\ln(\frac{2R}{l_p})} \quad (11)$$

Finally divide the force equation by the diffraction index since the speed is reduced to  $c/n$  where  $n = \sqrt{\epsilon}$  which is the diffraction index of low-density polyethylene (LDPE) plastic or mylar. Drop the approximation for simplicity.

$$\Delta F_e = \frac{2hc}{\sqrt{\epsilon}d^2} \frac{\ln(\frac{R}{d})}{\ln(\frac{2R}{l_p})} \quad (12)$$

The above results in the theoretical model for the force seen on one electron accelerated mass. Finally multiply by the number of electrons  $N_e$  to find the total force on the capacitor.

$$\Delta F = \frac{2hcN_e}{\sqrt{\epsilon}d^2} \frac{\ln(\frac{R}{d})}{\ln(\frac{2R}{l_p})} \quad (13)$$

## 4.2 Theoretical force model by Wave energy formula

One can also derive the theoretical model of the force by using the wave energy formula.

$$E = \frac{hc}{\lambda} \quad (14)$$

Now let us find the total wave energy in the confinement region letting  $\lambda = kl_p$  to count all the waves up to  $N$ . Here the  $l_p$  comes from the fundamental wavelength.

$$\sum_{k=1}^N \Delta E_d = \frac{hc}{l_p} + \frac{hc}{2l_p} + \dots + \frac{hc}{Nl_p} \quad (15)$$

Plug in for  $\lambda = kl_p$  in order to count all the waves in the Rindler region up to  $M$ .

$$\sum_{k=1}^M \Delta E_R = \frac{hc}{l_p} + \frac{hc}{2l_p} + \dots + \frac{hc}{Ml_p} \quad (16)$$

Now compute the ratio of fractional energy that will be pushing the capacitor. Namely, the ratio  $\frac{\Delta E_R - \Delta E_d}{\Delta E_R}$ .

$$\frac{\Delta E_R - \Delta E_d}{\Delta E_R} = \frac{\left(\frac{hc}{l_p} + \frac{hc}{2l_p} + \dots + \frac{hc}{Ml_p}\right) - \left(\frac{hc}{l_p} + \frac{hc}{2l_p} + \dots + \frac{hc}{Nl_p}\right)}{\frac{hc}{l_p} + \frac{hc}{2l_p} + \dots + \frac{hc}{Ml_p}} \quad (17)$$

Now write the equation in closed form and simplify. Notice the common terms will factor out and cancel and will be the same result as (5).

$$\frac{\Delta E_R - \Delta E_d}{\Delta E_R} = \frac{\sum_{k=1}^M \frac{1}{k} - \sum_{k=1}^N \frac{1}{k}}{\sum_{k=1}^M \frac{1}{k}} \quad (18)$$

Follow the steps in previous derivation to finally result in the following with the only difference being the force is over the entire confinement region,  $d$  and not  $0.5d$ .

$$\Delta F = \frac{2hcN_e}{\sqrt{\epsilon}d^2} \frac{\ln\left(\frac{R}{d}\right)}{\ln\left(\frac{2R}{l_p}\right)} \quad (19)$$

In general, the overall force will be established by multiplying the force of a single acceleration event with the number of particles (electrons) involved over the duration of one second as determined by the electric current flow (total burst amount of accelerated particles.) For the stacked capacitor, the overall force corresponds to the multiplication of the number of particles times the number of acceleration stages. Essentially, this is the force times the overall number of accelerated events within one second.

## 5 Discussion

While conducting a variety of capacitive discharge experiments from 2017-2019, a directional force was repeatedly observed during field emission and insulation breakdown discharge of parallel capacitive charged plates.

The collected experimental data highlighted:

1. A linear correlation between the thrust force and the accelerated mass.

2. An exponential increase in the observed force with the decrease of the capacitor electrode distance, while keeping the accelerated mass constant.

The effect was only observable and repeatable under certain conditions:

1. With a very short capacitor plate separation distance.
2. Under a uniform discharge causing the acceleration of only electrons (as the charged accelerated particles).

It appears that if an electric discharge occurs, such as bridging the electrodes by arcing, this would introduce positive charges to the system which would hinder the effect. Additionally, the force appears reversible when conductive material, insulated from the cathode, is inserted right behind the cathode of the capacitor, thus behind the accelerated electrons. Furthermore, placement of the conductive material past the rindler horizon,  $R$ , also changes certain behaviors of directional force depending on if the material is connected to the cathode or not. Finally, extending the cathode thickness, between  $R$  and the cathode, can also decrease the normal effect. Similar testing was conducted adding conductive material in front of the anode. This led to the same results as without the attenuation material (equal to original effect).

A simulation of a physical model was refined allowing the prediction of the measured force values by using aspects of the uncertainty principle and concepts derived from the theory of quantised inertia. This was done using a simple equation associated with virtual particles (photons, Unruh radiation) derived from the information boundary of a Rindler horizon and the information deflection scenario of the anode inside the electron propagation path introducing an energy gradient. In the experiment, this would have to be sufficiently high to become observable.

The present results, due to the clear operational characteristics of the trend lines and 507 data points collected, allow for the positive identification of a new effect. The prototype thruster concepts can be modeled with an equation based on some concepts as outlined by theory of quantised inertia [7] [8] using (discrete) Unruh waves with nodes at the horizon. Since the predictive model and the experimental results are very closely converging, and no other models exist explaining the effect without violating the present law of physics, the result may also denote that an Unruh-like radiation exists.

From all four sub-experiments, it is proposed that confined Unruh radiation is composed of a discrete spectrum. This particular confinement scenario and the causal information confinement by a Rindler horizon can be used for practical applications. The experiment has shown that a Rindler horizon physically exists. Additionally, an associated horizon radiation may cause an alteration in the energy state distribution of virtual particles and, in turn, provides a means to modify accelerative conditions. This may provide the basis to further conclude the actual existence of an Unruh-like radiation condition. Furthermore, as the identified thrust force acts in the general inertial framework, this experiment may provide the basis of certain aspects of the theory of quantised inertia.

With regards to the topic of a discrete Unruh radiation in the confinement by the

anode, it could be speculated that this is caused by the end of the field lines on an electrical horizon. For example, the accelerated electrons have their own wavelength for which the thickness of the anode material would disallow the penetration. Therefore this limits the possible interaction of the electrons and their forward path world line and they would experience full attenuation as seen in particle/wave duality. Furthermore, Unruh radiation photons, which are experienced by the electrons, would not be able to penetrate through the anode plate thickness so the Unruh waves, which are able to propagate in the seeing zone, would be virtual particles created at the location of the anode. This also suggests that the anode may operate for the accelerated electrons as a causal event horizon equivalent. The results of this experiment suggest further research on this mechanism is recommended, namely, inspecting the physical feature of the anode which could act as an information horizon which appears to be observable. Additionally, artifacts are considered to be of a low probability due to the merging trend lines with different experimental setups. This would exclude the fact that two different artifact disturbances could provide data points on the same curve for the device.

In another view, one could consider the inside zone between the cathode and anode to be correlated to the conventional Casimir effect. An electron immersed in this quantum state environment, having an acceleration and by that a Rindler horizon, would be under the influence of an additional field which corresponds to the radiation emitted by the Rindler horizon (reference to the initial hypothesis of Unruh radiation). Hence, the electron might be under the influence of two overlapping fields of quantum states. This would provide an energy/momentum gradient in the fields which, by conservation of momentum law, would initiate a resulting force effect due to the natural symmetry breaking by altering the normal natural radiation which is causing inertia. The electron floats inside a casimir scenario in between the electrodes. Here, the radiation difference around the electron is not homogenous compared to the normal Casimir effect. Rather the addition of the Rindler horizon radiation causes it to become inhomogeneous.

The new battery-powered onboard wireless setup resulted in successful for bi-directional thrust. A thrust to approximately 10 mg was commonplace for our 20um capacitor with shunt currents matching the wired setup. Earth's magnetic field which was around 45uT (measured) and an overestimate max length of 0.5 m for supply wires with a draw current of 0.5A in the primary circuit (measured and specs). Additionally, the wires ran vertically and twisted so would unlikely result in any appreciable Lorentz forces. Even in a theoretical maximum scenario the influence would be in the 1 mg range and should not affect the overall plausibility of the results. Additionally, a large magnet was placed in the vicinity of the DC wires and there was no noticeable effect during operations. Seems magnetic fields do not have much of an impact as expected for the vertically twisted wires on the scale values. Furthermore, the capacitor device direction was flipped without any change to DC circuit wiring so therefore any Lorentz forces would be always in one direction.

In regards to a prototype thruster (quantum vacuum thruster), evidence collected would support the claim that the construction of a modular capacitor system, scalable and with relatively low power consumption, could be indeed feasible. The prototypes in this paper have a performance above 0.4 N/kW. This is a performance that Dr. H. White (NASA's SSRMS Subsystem Manager) considers as a minimum requirement

for a crewed mission to Titan/Enceladus [14]. Construction of modular stacked segments could also provide the advantage of individual segment shut-down in case of failure/malfunction, without compromising the thrust performance of the remaining part of the capacitors. Since the thruster concept is exclusively electric, this experimental discovery could provide a first tangible mean for interstellar space exploration once an adequate source of energy is fine-tuned (see performance chart Fig. 9.)

## 6 Conclusion

By conducting tests on capacitive systems which accelerate electrons at values on the order of magnitude of  $10^{19}$  [ $\text{m s}^{-2}$ ] during field emission, a force accelerating the overall system has been clearly identified and characterized. This thrust force, observed distinctively in capacitors with a minimized distance between the electrodes, is in linear correlation with the amount of accelerated matter, which corresponds to the electrons released through an electric current determined by field emission. The force occurs when the causal propagation zone is confined to less than 50% of the acceleration associated with the Rindler horizon distance. The force is directed in the propagation direction, but can be reversed by attenuating the associated horizon boundary (Unruh) radiations within the Rindler zone. This can be done by placing conductive material at specific distances in the area behind the cathode (thus outside the capacitor). In these instances, the attenuator is electrically insulated from the cathode. Additionally, extending the cathode decreases the normal force proportionally by distance and can also create a force reversal if extended past the Rindler horizon.

Throughout the experimental tests it was identified that the force increases exponentially when distance between electrodes is decreased. The force detection was confirmed in soft vacuum condition as well, showing evidence of lower standard deviation of the collected data. It is also worth mentioning that the observed phenomenon does not seem correlated with evidence collected while testing ion lifters [10]. The “thrust anomaly”, in fact, is assumed to be caused by electrons accelerated within a capacitor due to a field emission from a high electric field. To observe this thrust, it is paramount to keep the distance between the electrodes at minimum.

The observed thrust can be enhanced by preheating the capacitor so that the energy value required by the electric field for electron transmission can be lowered by means of Schottky/thermionic effects. In addition, the field strength can be increased by changing the field type from homogeneous to inhomogeneous. For instance using sandpaper or applying a high number of small cuts on the cathode surface can facilitate field emission. Furthermore, the force can be multiplied by using a modular design of stacking capacitors in series: this architecture, with respect to a single, higher performing capacitor, has the advantage of keeping each segment performance independent from the remaining ones.

The indirect discovery of the existence of Unruh radiation (or some other oscillatory nodal waves with information boundaries within the zero point field of virtual particles, abbreviated suggested as QVO “quantum vacuum oscillations”) demonstrates a net force in accordance to a physical model aligned with core concepts initially outlined by McCulloch’s theory of quantised inertia. The experiment has shown that a Rindler horizon physically exists and this horizon radiation provides a means to mod-

ify accelerated conditions.

The capacitors tested in the experiments have a performance above 0.4 [N/kW]; a benchmark often used by NASA to define a thrust ratio sufficient for interplanetary travel. This simple technology, in fact, has the advantage of being completely electric, thus suitable for fuel-less electric propulsion in vacuum. Moreover the scalability of this architecture, coupled with adequate energy source generation, might be appropriate for interstellar travel and precise maneuvering in space.

Looking into the trend results of the conducted experiments, it should be seen essential to conduct the experiment with more accurate calibrated measuring equipment. It is also suggested that next scientific efforts should focus on correlating these results with an existing theoretical framework, so that an apparent anomaly can be adequately predicted and controlled for practical engineering purposes. The preliminary correlation results are certainly encouraging. A second priority would be to test and/or prepare this apparatus in space to validate its performance in a vacuum and its performance away from a strong gravity source.

## 7 Acknowledgments

We would like to express gratitude to the persons who assisted in the development of the experiment and as well as the facilitation for the results and compilation of this document. In particular we would like to thank Prof. Dr. M.E. McCulloch for encouraging us and providing us directions. Furthermore, we would like to thank Prof. Dr. M. Tajmar for his advice during experimentation. For supporting us in the setup of our early experimental stage, we would like to say thank you to Tommy Callaway. Furthermore, we appreciate the open minded discussions with John Doorman and Fabio Zagami on many general related subjects. Finally, this research would have never taken place if F.W. Becker would have not, decades ago, supported one of the authors (his son) and provided him the first means to see the initial observation of the effect in a science laboratory. The authors would like to express gratitude to both their families for supporting their academic endeavors.

## 8 Appendix A: Alternate Theoretical Model

Here, inspect the seeing zone conditions where the more precise seeing zone length is (with  $\beta = 0.2014$  pers. comm. McCulloch) and  $4\beta\pi^2 = 7.951$ . For simplification consider the maximum wavelength as suggested by McCulloch as approximately 8 Rindler distances. Basically 7 more oscillations compared to the fundamental wavelength of the Rindler zone are allowed inside the propagation path. Using (1) this results in the approximated unshared wave energy level simplified to:

$$\sum_{k=1}^{8-1} \frac{k}{8R} hc \quad (20)$$

Here,  $R$  is the Rindler distance. From computing the sum, this yields an approximate constant factor of  $6.925 * 10^{-25}$  [J m] which can be multiplied with  $1/R$  to determine the delta energy of the un-attenuated accelerated inertial condition (by considering the contribution of the unshared waves.) Let us call this parameter, since it is relevant for a 1 meter definition for the time being, the inertial energy factor due to the dimensional unit of [J m].

The quantised seeing zone energy of the unshared oscillations would require the equilibrium to cross the abscissa  $x$ -axis at one Rindler distance. Furthermore, in the un-attenuated confined state, the energy level at  $8R$  should be the same as computed by the inertial energy factor for the inertial undamped state. In this case, the number of allowed unshared waves is 7 which is used for the total summation function.

For curve fitting, the following equation can be created to match the seeing zone equation for a general  $x = R$  situation to find the constant 7.111 by adjusting the output value to the same value as the 'inertial energy' factor for 1 meter. Basically, this is accomplished by setting the confinement length to  $d = 8$  Rindler lengths.

$$\Delta E = \sum_{k=1}^7 \left( \frac{8-1}{8^2} \right) \frac{7.111k}{8} hc = 6.925 * 10^{-25} \quad (21)$$

The numerical determination of the seeing zone energy factor will be  $7.111/8$ . Below the number of unshared waves can be computed by a integer variable that is dependent on the ratio  $d/R$ .

$$\Delta N = \lceil 7.5 - \left( \frac{7}{1} - \frac{d}{R} \right) \rceil \quad (22)$$

Now one can replace the value 8 in (23) with a more general confinement position  $d$  to find energy behavior over the change in the confinement distance while still keeping the previous numerical; estimated seeing zone related energy factor of  $1/1.125$ .

$$\Delta E = \sum_{k=1}^{\Delta N} \left( \frac{d-R}{d^2} \right) \left( \frac{7.111k}{8R} \right) hc \quad (23)$$

The overall situation can be represented by the following.

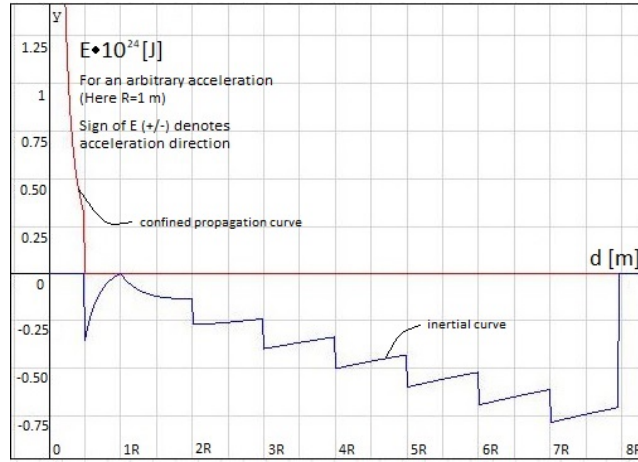


Figure 26: Approximation of energy delta profile in confined seeing zone

By the engineering approach of curve fitting between the 2 extrema of the zero cross equilibrium at  $1R$  and the un-attenuated original inertia situation energy level at approximately  $8R$ , it appears that the identified fitting parameter of  $7.111/8$  would refer to the factor  $1/1.125$  which corresponds to the increase in the original wave energy of the individual steps up to the point where the one wavelength is cancelled out (by reduction of confinement distance). Notice the overall curve is valid for a confinement  $d > 0.5R$ .

In Fig. 26 at a given Rindler length inside the propagation path, a confinement situation is established which reduces the quantised wavelength in front of an accelerated particle.

An interesting note is that between  $0.5R$  and  $1R$  the absolute energy delta is increasing with the further reduction of confinement length. This correlates to the situation where the energy in the Rindler zone is constant and the same wave number in the propagation path exists, but due to shorter confinements, a slightly shorter wavelength (as limited by the maximum allowed fundamental wavelength and the compulsory nodes at the boundaries) provides a higher energy level in the confinement zone. This continues until a confinement position of  $0.5$  Rindler length, where the fundamental wavelength is cancelled.

Fig. 26 does not include the consideration that all wavelengths in the confinement are shorter, with regards to the respective count compared to all allowed wavelengths in the Rindler zone (as this only focuses on the unshared wavelength contribution to the energy delta). Hence, this is simply a first illustration of the energy profile in a case where the seeing zone confinement is applied.

## 9 Appendix B: Skin Depth

Below is the simplified skin depth equation for good conductors.

$$\delta = \sqrt{\frac{2\rho}{2\pi f \mu_r \mu_0}} \quad (24)$$

$\rho$  = resistivity of the conductor

$f$  = frequency of current

$\mu_r$  = relative magnetic permeability of the conductor

$\mu_0$  = the permeability of free space

## 10 Appendix C: Potential Errors

The results during both the remote (battery powered unit without exposed HV conductors) and wire testing could result in “Trichel pulses” by insufficient insulation. The signature of these pulses have the properties of lifted currents (offset = DC component with sharp inrush currents) as seen on the oscilloscope display. The signals look similar to field emission currents but have different attributes (spikes), and are actually a corona discharge with trichel pulses. Field emission events occur having current peaks starting from approximately zero on the display of the oscilloscope. In contrast, external located trichel impulses (in wiring etc.), which are generated outside the test capacitor, do fluctuate but are added in amplitude to the small DC component leakage current. It was found that a leakage current is likely generated from a conductive enclosure such as the Faraday shielding cage without sufficient inner insulation material near a thin high voltage charged conductor. Here, it would also be relevant to check the insulation rating when appropriate since, for example, a 500 V rating would be insufficient as a direct barrier between HV polarities. Usually, 500 V is a typical standard value rating of insulators on the market. Furthermore, an air layer with the insulation material of a conductor could become a composite capacitor (voltages distribute with each material index and per thickness involved). The electric field strength inside the air is significantly higher than inside the material. Therefore if a metallic object, such as a shielding enclosure, is connected to the negative polarity, electrons could be tunneled out the surface due to insufficient insulation and ionize the air gap to the next conductor. Additionally, using conductors not rated appropriately to the intended use could also lead to a null effect due to leakage currents. Additionally, having twisted conductor supplies inside sheeted routing should not be near the enclosure which could have a different polarity. If the field is strong enough the electrons could be pulled out of the enclosure and accelerated towards the insulator.

One can also consider the influence of possible Lorentz forces even though the HV supply current is significantly low. One solution is the usage of twisted conductors. However, this should be done with care as twisted conductors with different polarities with longer lengths could also cause leakages. Hence it should be seen essential to provide twisting with limited/avoiding direct contact of insulation of conductors with different polarities during a high voltage scenario. During twisting, application of air loops may boost insulation distance and limit the direct contact points. Also, it is necessary to utilize conductors rated for the high voltage application. Adding tubing over high voltage conductors rated up to 500V (working voltage, insulation voltage) should be considered an insufficient insulation system if there is direct contact with one

conductor (Faraday or conductive mu-metal surface connected to one HV polarity). Recreation of the Trichel pulses during were performed in January 2019 during further testing. The result usually ended in a null effect since the path of least resistance was not through the capacitor. Larger currents around 10uA were commonplace measured at the shunt. For a valid effect, values were nominally much lower in the low uA range for a large normal effect.

At the current state of research it is not yet clarified whether the quantum vacuum oscillations emerge from the local vacuum or are emitted by the cosmic horizon [7]. A mu-metal shielding might cause complications during testing so in the future it is suggested to compare the use of normal Faraday cages and mu-metal cages.

## References

- [1] A. Froebel. Cable shielding to minimize electromagnetic interference. *EEEIC*.
- [2] D. Go and D. A. Pohlman. A mathematical model of the modified paschen's curve for breakdown in microscale gaps. 107:103303 – 103303, 06 2010.
- [3] S. Harjo. Partial discharge in high voltage insulating materials. 8:147–163, 03 2016.
- [4] S. W. Hawking. Evaporation of two-dimensional black holes. *Phys. Rev. Lett.*, 69:406–409, Jul 1992.
- [5] Y. Lau and Y. Liu. From fowler-nordheim relation to the child-langmuir law. 1994.
- [6] M. McCulloch. Inertia from an asymmetric casimir effect. 101, 02 2013.
- [7] M. McCulloch. Low-acceleration dwarf galaxies as tests of quantised inertia. 362, 03 2017.
- [8] M. E. McCulloch. Minimum accelerations from quantised inertia. *EPL (Europhysics Letters)*, 90(2):29001, 2010.
- [9] E. L. Murphy and R. H. Good. Thermionic emission, field emission, and the transition region. *Phys. Rev.*, 102:1464–1473, Jun 1956.
- [10] M. Tajmar. Biefeld-brown effect: Misinterpretation of corona wind phenomena. *AIAA Journal*, 42(2):315–318, Feb 2004.
- [11] R. L. Talley. Twenty First Century Propulsion Concept. Technical Report F04611-89-C-0023, VERITAY TECHNOLOGY INC, May 1991.
- [12] W. Unruh. Acceleration radiation for orbiting electrons. 307:163–171, 04 1998.
- [13] W. G. Unruh. Notes on black-hole evaporation. *Phys. Rev. D*, 14:870–892, Aug 1976.
- [14] H. G. White. Q thrusters. In *Pilot Wave Model for Impulsive Thrust from RF Test Device*, Breakthrough Discuss - Day Two, 2018.